
CONDENSED
MATTER

Wannier Diagrams for Semiconductor Artificial Graphene

O. A. Tkachenko^{a, *}, V. A. Tkachenko^{a, b}, D. G. Baksheev^b, and O. P. Sushkov^c

^a *Rzhanov Institute of Semiconductor Physics, Siberian Branch, Russian Academy of Sciences,
Novosibirsk, 630090 Russia*

^b *Novosibirsk State University, Novosibirsk, 630090 Russia*

^c *University of New South Wales, 2052 Sydney, Australia*

**e-mail: otkach@list.ru*

Received September 19, 2022; revised September 19, 2022; accepted September 21, 2022

Quantum transport has been simulated in hexagonal semiconductor lattices of antidots with a period of 80 nm and short-range disorder. Wannier diagrams, i.e., $DoS(n, B)$ maps of the density of states, where n is the electron density and B is the magnetic field strength, have been calculated for several potential modulation amplitudes comparable to or much larger than the Fermi energy. Deep dips in the maps of the density of states have the form of rays with positive, zero, and negative slopes. In addition to the fan of the rays separating the first and second, as well as the second and third Landau levels, the maps include rays that are parallel to them and are shifted in n and B by integers of the characteristic electron density n_0 and the characteristic magnetic field strength B_0 , respectively. It has been shown that the sign and magnitude of the slope of the rays in the density of states correspond to the centers of the plateaus of quantized Hall resistances R_{xy} . The lattice is brightly manifested in the $R_{xy}(n, B)$ maps as the replicas of the first and second plateaus in R_{xy} and as oscillations of R_{xy} between negative and positive values at a fixed magnetic field or a fixed electron density, which indicates the interchange between the hole and electron charge carriers.

DOI: 10.1134/S0021364022602020

Artificial materials and systems similar to natural graphene with a Dirac cone in the dispersion relation but in a different range of the parameters are currently fabricated and studied [1–4]. Hexagonal lattices of antidots with a period of 80–120 nm, which are formed nanolithographically in a high-mobility two-dimensional electron gas of GaAs/AlGaAs heterostructures, are called semiconductor artificial graphene [4, 5]. Semiconductor artificial graphene has two interesting Dirac points: the first point appears at the crossing of the two lowest minibands, and the second occurs at the intersection of the fourth and fifth minibands [6–9]. It was shown that Landau–Dirac quantization in the absence of disorder occurs near a Dirac point in very weak magnetic fields $B < 10$ mT [5]. However, Dirac points in quantum transport in semiconductor artificial graphene have not yet been detected. The main reason is disorder [9, 10], and the existence of Dirac points in semiconductor artificial graphene is currently indicated only by the study of photoluminescence at interband transitions in a GaAs quantum well at $B = 0$ [4]. Nevertheless, manifestations of the magneto-electric miniband spectrum of the lattice or the Hofstadter butterfly [11] were detected on a square lattice with a period of about 100 nm, when the Fermi energy E_F was much higher than the modulation amplitude V [12]. A nonmono-

tonic behavior of the Hall resistance was observed for high Landau levels; disorder was well screened in this case.

The height of potential barriers at antidots should be much higher than the Fermi level for a pronounced Dirac cone to appear in semiconductor artificial graphene. The effect of disorder in this case becomes strong and can destroy the Dirac point [9]. Measurements show that observed effects depend on the amplitude of periodic modulation [13]. In particular, only effects of magnetic breakdown are observed at weak modulation [14, 15], and they disappear with increasing modulation amplitude. According to the calculation of quantum transport in semiconductor artificial graphene disregarding disorder, plateaus of the hole and electron conductivities are formed below and above the zeroth Landau level in the electron density at low magnetic fields [5]. Magneto-electrical minibands and edge states in semiconductor artificial graphene at high magnetic fields have recently been simulated disregarding disorder [16]. The integral effect of the lattice can be revealed from $DoS(n, B)$ maps of the density of states, i.e., Wannier diagrams, where n is the charge carrier density and B is the magnetic field [17]. In particular, this concerns the experimentally studied graphene superlattices, which have a period of about 15 and 35 nm and demonstrate the

cloning of the main Dirac point and Hofstadter butterfly [1–3].

In this work, we present Wannier diagrams calculated for various modulation amplitudes of the semiconductor lattice of antidots taking into account short-range disorder. The calculations of the Hall resistance R_{xy} show a close relation between $DoS(n, B)$ and $R_{xy}(n, B)$ maps. Calculated maps of the density of states can allow one to forecast the measurement results and to estimate real modulation and disorder levels.

The calculations were performed with the analytically specified potential $U(\mathbf{r}) = V_d(\mathbf{r}) + V_0 \sum \cos(\mathbf{g}_i \cdot \mathbf{r})$ of the hexagonal lattice with the period L on a $2-3 \mu\text{m}$ square, where V_0 is the amplitude of potential modulation, the function $V_d(\mathbf{r}) = V_r \delta$ with a random number δ ranging from -0.5 to 0.5 and the disorder amplitude V_r specifies a random addition to the potential of the lattice in each cell of the discrete lattice ($h_x = h_y = 8 \text{ nm}$) [15], and \mathbf{g}_i , $i = 1-3$, are the reciprocal lattice vectors given by the expressions

$$\mathbf{g}_1 = g_0(1, 1/\sqrt{3}), \quad (1)$$

$$\mathbf{g}_2 = g_0(0, 2/\sqrt{3}), \quad (2)$$

$$\mathbf{g}_3 = \mathbf{g}_1 - \mathbf{g}_2 = g_0(1, -1/\sqrt{3}), \quad (3)$$

where $g_0 = 2\pi/L$. It was shown in [9] that the band structure of the lattice depends only on the dimensionless amplitude of potential modulation $w_0 = 0.5V_0/E_0$, where $E_0 = \frac{8\pi^2}{9} \frac{\hbar^2}{m^* L^2}$ is the characteristic energy, which is equal to 1.56 meV for the effective mass of the electron in GaAs $m^* = 0.067m_e$ and the lattice period $L = 80 \text{ nm}$. At low modulation $w_0 < 1$, the third and higher minibands of the lattice are imposed on the second miniband. As modulation increases, minibands rise and are flattened, so that the third flat band and the second Dirac point are already formed at $w_0 = 1.5$ [9].

Lattices are described in terms of the characteristic carrier density $n_0 = 2/(\sqrt{3}L^2/2)$ corresponding to two particles per cell and the characteristic magnetic field B_0 at which the magnetic flux $\phi = B\sqrt{3}L^2/2$ through the cell of the lattice is $\phi_0 = h/e$. It is noteworthy that $n_0 = n_{1D}$, where n_{1D} is the carrier density at the first Dirac point. For the lattice period $L = 80 \text{ nm}$, $B_0 \approx 0.75 \text{ T}$ and $n_0 \approx 3.6 \times 10^{10} \text{ cm}^{-2}$.

The potential on the strip beyond the square region under consideration was assumed uniform and equal to the minimum potential of the lattice in the absence of disorder. Then, the problem of two-dimensional single-particle quantum scattering of electron waves incident on the mentioned square from the left and right was solved by the recursive Green's functions

method [18]. As a result, we obtained the local density of states as a function of the energy E and the magnitude B of the perpendicular magnetic field. The integration of $DoS(E)$ over a wide energy range up to E_F gives $n(E_F)$ at a given B value [19]. It was shown that the introduction of a small imaginary part of the energy in the definition of the Green's function makes it possible to effectively smooth interference oscillations in $DoS(E)$ without loss of the accuracy of calculation of the carrier density. The magnetic field B was additionally varied with a small step from 0 to 2 T corresponding to the quantum Hall effect. These calculations were carried out with the lattice period $L = 80 \text{ nm}$; the local disorder amplitude $V_r = 2 \text{ meV}$ for the modulation amplitudes $w_0 = 0.1, 0.25, 0.5$, and 1 ; and the local disorder amplitude $V_r = 5 \text{ meV}$ for the modulation amplitude $w_0 = 1.5$. As a result, we obtained $DoS(E, B)$, $DoS(n, B)$, and $E_F(n, B)$ maps.

Figures 1 and 2 show the corresponding maps, where the yellow and blue regions correspond to the maximum and minimum densities of states. These maps demonstrate transition from the fan of Landau levels (at $w_0 = 0.1$) to an almost periodic pattern (at $w_0 = 1$) in the region of low carrier densities ($n < 2n_0$) and low magnetic fields ($B < 2B_0$). In the calculations, the total modulation amplitude varied from 1.4 meV (at $w_0 = 0.1$) to 21.1 meV (at $w_0 = 1.5$) and the cyclotron energy $\hbar\omega_c$ varied from 0 to 3.46 meV at 2 T .

Modulation in the first two maps is comparatively weak and Landau levels (Shubnikov–de Haas oscillations) are manifested as maxima of the density of states. Dips in the density of states between them diverge as rays from the point $n = B = 0$ and correspond either to edge states (inclined lines), when electrons are absent inside the lattice and move only along the edge of the lattice, or to band gaps in the lattice (horizontal lines), when electrons do not enter the sample at all. The slope $k = \tilde{n}/\tilde{B}$ of dark lines in the dimensionless variables $\tilde{n} = n/n_0$ and $\tilde{B} = B/B_0$ is directly related to the quantized conductance $G = kG_0$, where $G_0 = 2e^2/h$, or the quantized Hall resistance $R_{xy} = R_0/k$, where $R_0 = 1/G_0$; dark lines determine the centers of quantized conductance or resistance plateaus. According to our calculations, the R_{xy} plateaus are always wider than dips in the density of states. Fans of rays on the (n, B) map of the density of states correspond to the formation of Landau levels from the miniband edges and originate from the (ln_0, mB_0) points, where l and m are integers.

An upward ray with a slope of $k = 1$ and a much less pronounced downward ray with a slope of $k = -1$ originate from the $(n_0, 0)$ Dirac point at $w_0 = 0.1$. The $(2n_0, B_0)$ and $(3n_0, B_0)$ points are the centers of rays with different slopes; a ray with a slope of $+1$ originates from the $(0, B_0)$ point. Lines parallel to the main rays separating Landau levels appear. For exam-

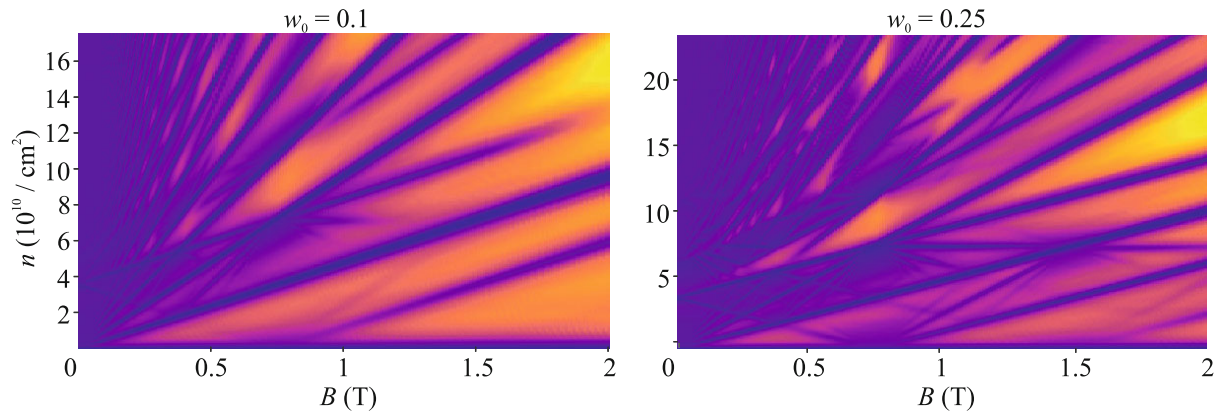


Fig. 1. (Color online) $DoS(n, B)$ maps for the lattice with the modulation amplitudes $w_0 = 0.1$ and 0.25 .

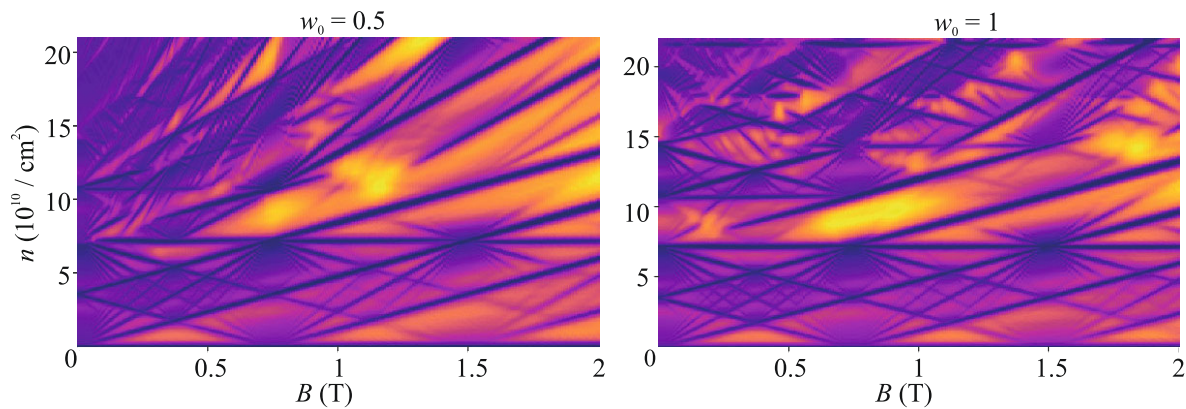


Fig. 2. (Color online) $DoS(n, B)$ maps for the lattice with the modulation amplitudes $w_0 = 0.5$ and 1 .

ple, a ray with a slope of $k = 2$, which enters the $(3n_0, B_0)$ point from above, can be continued down to the first Dirac point. The map of rays becomes more pronounced at $w_0 = 0.25$ and 0.5 . Since rays correspond to the centers of the Hall resistance plateaus, the quantum Hall picture should be very unconventional and should contain three or four replicas of the first $R_{xy} = R_0$ plateau. Although the dispersion relation for $w_0 = 0.1$ – 0.5 at $B = 0$ is gapless, a horizontal ray originating from the $(2n_0, B_0)$ point at $w_0 = 0.1$ – 0.25 continues toward low and high magnetic fields at $w_0 = 0.5$. The band gap can be washed out by disorder, but it is manifested in the calculations as a region of high resistances.

The band gap between the second and third minibands already exists at $w_0 = 1$ and is manifested as a horizontal ray originating from the $(2n_0, 0)$ point on the map of the density of states. The map for carrier densities below $2n_0$ is almost periodic in magnetic field with a period of B_0 . Two rays with slopes of $+1$ and -1 , as well as downward rays with slopes of -3 , -5 , and -7 , which indicate Landau–Dirac quantization, originate from the second Dirac point $(4n_0, 0)$. At higher

carrier densities, the clear pattern disappears because of the overlapping of different minibands of the lattice. The third (flat) miniband of the lattice has a high density of states and is manifested in the bright strip of the density of states beginning at the $(E = 2 \text{ meV}, B = 0)$

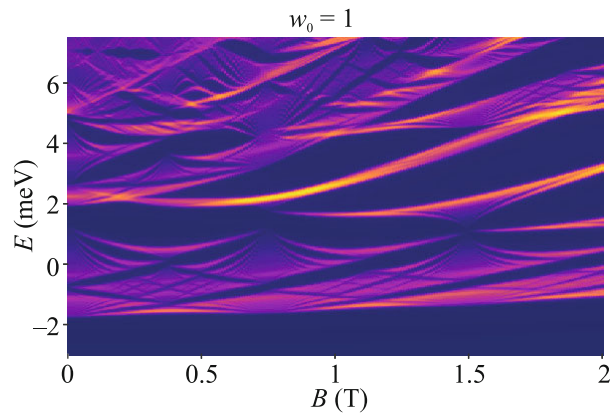


Fig. 3. (Color online) $DoS(E, B)$ map for the modulation amplitude $w_0 = 1$.

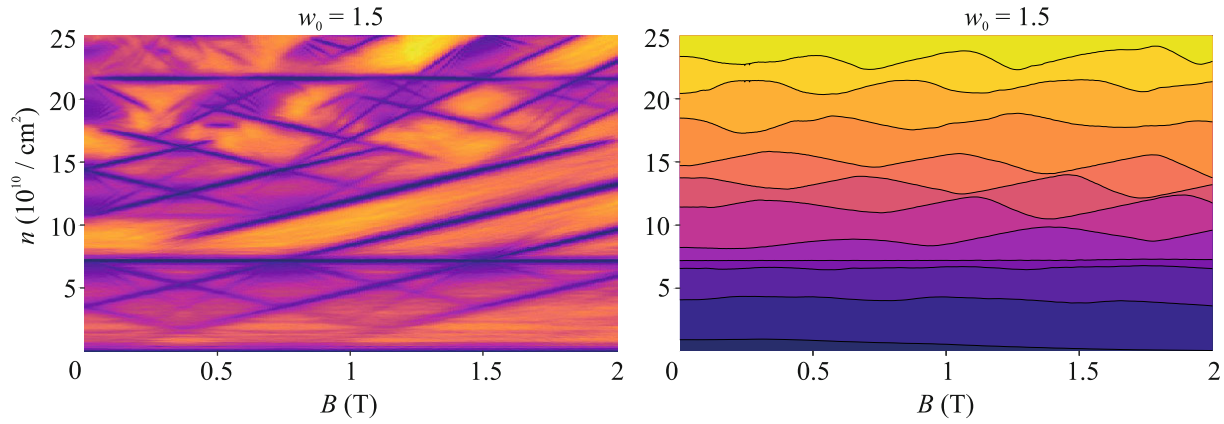


Fig. 4. (Color online) (Left) $DoS(n, B)$ and (right) $E_F(n, B)$ maps for the modulation amplitude $w_0 = 1.5$ at $V_r = 5$ meV.

point in Fig. 3. The $DoS(E, B)$ map is similar to the Hofstadter butterfly, which was calculated in almost three B_0 periods for a finite lattice with a total modulation of 14 meV taking into account disorder. When the energy is recalculated to the corresponding carrier density, regions with a low density of states are contracted to narrow strips, whereas regions with a high density of states are expanded; as a result, the entire curved $DoS(E, B)$ map is straightened out to a series of rays on the (n, B) plane (analog of the Wannier diagram).

An additional horizontal line at a carrier density of $n = 6n_0 = 21.65 \times 10^{10} \text{ cm}^{-2}$ appears in Fig. 4 at $w_0 = 1.5$ after filling of six minibands in the magnetic field. Strong disorder with the amplitude $V_r = 5$ meV washes out the fine structure of the density of states. Rays with slopes of $+1$ and -1 dominate, whereas the fan of conventional Landau levels disappears. The right panel of Fig. 4 shows the $E_F(n, B)$ map, where color varies from dark blue corresponding to -4 meV to yellow for 8 meV. The function $E_F(n = \text{const}, B)$ is an almost periodically oscillating function.

Hall resistances were calculated using the Kwant software package [20] with the potential and disorder defined with the same formulas as before. The calculation was performed in the four-terminal configuration: two horizontal channels through which electron scattering occurs are connected to the left side of the square with the lattice, at top and bottom, and to the right side of it. Four-terminal resistances were reconstructed by Büttiker formulas [21] from the calculated transmission coefficients between terminals in the system.

Figure 5 shows the magnetic field dependence of the Hall resistance calculated at a carrier density of $n = 6 \times 10^{10} \text{ cm}^{-2}$, a disorder amplitude of $V_r = 2$ meV, and three modulation amplitudes. As the magnetic field increases, the Hall resistance $R_{xy}(B)$ successively intersects strips of dips of the density of states with

slopes of $+1$ and -1 , demonstrating a sawtooth behavior. The $R_0/2$ and $R_0/3$ plateaus are not seen because they are narrow. The ranges of a negative Hall resistance indicate a hole conductivity. The behavior of $R_{xy}(B)$ correlates with $DoS(n, B)$ maps and becomes more pronounced with increasing modulation amplitude. The $R_{xy}(B)$ curve at $w_0 = 1.5$ passes through zero almost exactly at $jB_0/2$, where $j = 1-5$. In addition, it is remarkable that even strong short-range disorder taken into account in our calculations does not destroy quantized Hall resistance plateaus. Long-range disorder, which is due to slightly different sizes of holes in the gate specifying the lattice of antidots, provides a much stronger effect. Our calculations show that this disorder destroys the quantization of the Hall resistance at low magnetic fields $B < B_0/2$ (R_{xy} values decrease, but the sign holds) and suppresses lattice effects in high magnetic fields $B_0 < B < 3B_0$.

To summarize, the $DoS(E, B)$, $DoS(n, B)$, and $E_F(n, B)$ maps of semiconductor artificial graphene have been calculated for potential modulation ampli-

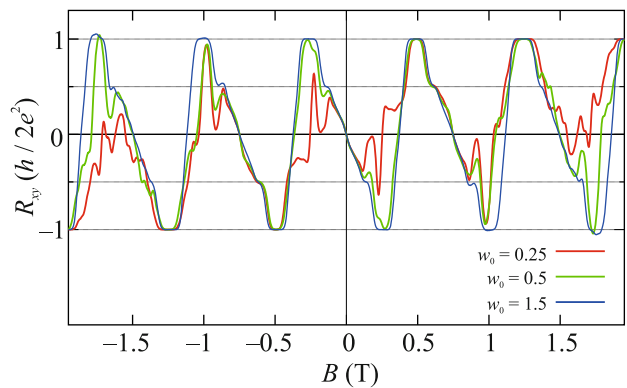


Fig. 5. (Color online) Magnetic field dependence of the Hall resistance $R_{xy}(B)$ calculated for $w_0 = 0.25, 0.5$, and 1.5 at a carrier density of $n = 6 \times 10^{10} \text{ cm}^{-2}$ and $V_r = 2$ meV.

tudes comparable to or much larger than the Fermi energy. These maps illustratively and deeply represent the Landau–Dirac quantization, Hofstadter butterfly, and magneto-electric oscillations of the Fermi level. It has been shown that the fan of Landau levels on the (n, B) maps is transformed with increasing lattice modulation to a rhombic structure formed by a set of parallel rays with different slopes of opposite signs. The feature of semiconductor artificial graphene is the alternation of hole and electron charge carriers; as a result, the Hall resistance $R_{xy}(B)$ oscillates between negative and positive values. The simulation results can contribute to the interpretation of measurements of the magnetotransport in lattices, e.g., Wannier diagrams, which were obtained by capacitive measurements of the density of states in short-period graphene superlattices [2, 3].

ACKNOWLEDGMENTS

We are grateful to O. Klochan, D.Q. Wang, Z.E. Krix, and A.R. Hamilton (University of New South Wales, Sydney, Australia) for stimulating discussion. We acknowledge resources provided by the Joint Supercomputer Center, Russian Academy of Sciences.

FUNDING

This work was supported by the Russian Science Foundation, project no. 19-72-30023.

CONFLICT OF INTEREST

The authors declare that they have no conflicts of interest.

OPEN ACCESS

This article is licensed under a Creative Commons Attribution 4.0 International License, which permits use, sharing, adaptation, distribution and reproduction in any medium or format, as long as you give appropriate credit to the original author(s) and the source, provide a link to the Creative Commons license, and indicate if changes were made. The images or other third party material in this article are included in the article's Creative Commons license, unless indicated otherwise in a credit line to the material. If material is not included in the article's Creative Commons license and your intended use is not permitted by statutory regulation or exceeds the permitted use, you will need to obtain permission directly from the copyright holder. To view a copy of this license, visit <http://creativecommons.org/licenses/by/4.0/>.

REFERENCES

1. L. A. Ponomarenko, R. V. Gorbachev, G. L. Yu, et al., *Nature* (London, U.K.) **497**, 594 (2013).
2. G. L. Yu, R. V. Gorbachev, J. S. Tu, et al., *Nat. Phys.* **10**, 525 (2014).
3. C. Forsythe, X. Zhou, K. Watanabe, T. Taniguchi, A. Pasupathy, P. Moon, M. Koshino, P. Kim, and C. R. Dean, *Nat. Nanotechnol.* **13**, 566 (2018).
4. L. Du, Z. Liu, S. J. Wind, V. Pellegrini, K. W. West, S. Fallahi, L. N. Pfeiffer, M. J. Manfra, and A. Pinczuk, *Phys. Rev. Lett.* **126**, 106402 (2021).
5. O. A. Tkachenko and V. A. Tkachenko, *JETP Lett.* **99**, 204 (2014).
6. C.-H. Park and S. G. Louie, *Nano Lett.* **9**, 1793 (2009).
7. M. Gibertini, A. Singha, V. Pellegrini, M. Polini, G. Vignale, A. Pinczuk, L. N. Pfeiffer, and K. W. West, *Phys. Rev. B* **79**, 241406(R) (2009).
8. L. Nádvorník, M. Orlita, N. A. Goncharuk, L. Smrčka, V. Novák, V. Jurka, K. Hruška, Z. Výborný, Z. R. Wasilewski, M. Potemski, and K. Výborný, *New J. Phys.* **14**, 053002 (2012).
9. O. A. Tkachenko, V. A. Tkachenko, I. S. Terekhov, and O. P. Sushkov, *2D Mater.* **2**, 014010 (2015).
10. O. A. Tkachenko and V. A. Tkachenko, *Vestn. Novosib. Univ., Ser.: Fiz.* **11**, 80 (2016).
11. D. R. Hofstadter, *Phys. Rev. B* **14**, 2239 (1976).
12. C. Albrecht, J. H. Smet, K. von Klitzing, D. Weiss, V. Umansky, and H. Schweizer, *Phys. E (Amsterdam, Neth.)* **20**, 143 (2003).
13. D. Q. Wang, D. Reuter, A. D. Wieck, A. R. Hamilton, and O. Klochan, *Appl. Phys. Lett.* **117**, 032102 (2020).
14. C. Albrecht, J. H. Smet, D. Weiss, K. von Klitzing, R. Hennig, M. Langenbuch, M. Suhrke, U. Rössler, V. Umansky, and H. Schweizer, *Phys. Rev. Lett.* **83**, 223470 (1999).
15. J. Schluck, J. Feilhauer, K. Pierz, H. W. Schumacher, D. Kazazis, U. Gennser, and T. Heinzel, *Phys. Rev. B* **98**, 165415 (2018).
16. Z. E. Krix and O. P. Sushkov, *Phys. Rev. B* **101**, 245311 (2020).
17. G. H. Wannier, *Phys. Status Solidi B* **88**, 757 (1978).
18. A. Cresti, R. Farchioni, G. Grosso, and G. P. Parravicini, *Phys. Rev. B* **68**, 075306 (2003).
19. O. A. Tkachenko, V. A. Tkachenko, D. G. Baksheev, and O. P. Sushkov, *JETP Lett.* **112**, 186 (2020).
20. C. W. Groth, M. Wimmer, A. R. Akhmerov, and X. Waintal, *New J. Phys.* **16**, 063065 (2014).
21. M. Büttiker, *Phys. Rev. Lett.* **57**, 1761 (1986).

Translated by R. Tyapayev